MINAR International Journal of Applied Sciences and Technology
ISSN: 2717-8234
Article type: Research Article

Received: 25/12/2023 **Accepted:** 06/02/2024 **Published:** 01/03/2024

EFFECT OF CeO2 NANOPARTICLES ON THE STRUCTURAL AND OPTICAL PROPERTIES OF (SnO2:Pd) FILMS PREPARED BY PLD TECHNIQUE

Ahmed Sh. MAHMOOD [1]
University of Baghdad, Iraq

Ghuson H.MOHAMMED [2]
University of Baghdad, Iraq

Abstract:

In this paper, pure and doped (SnO2:Pd) films with CeO2 nanoparticles prepared by PLD technique using a highly intense Nd:YAG laser beam at 600 mJ with a frequency of second radiation at 1064 nm (pulse width 9 ns) repeating frequency (6 Hz) for 400 laser pulses incident on the intended surface has been performed. The stabilized (SnO2:Pd) doped with cerium oxide were used for deposition of the thin films on glass with thickness 200nm±05. Films of SnO2:pd were prepared with different doping concentrations of CeO2(0, 0.05, 0.10,0.15,0.20 and 0.25) wt. The FTIR and UV-Visible spectrophotometer were employed to investigate the structural, and optical characteristics of the films, respectively. FTIR spectra of (SnO2:Pd)1-xCeO2x thin films show seven peaks were assigned at wavenumber range from 2869.73 cm-1 belong to stretching bond CH2 to 492.98 cm-1 belong to N-O which can be indicated by the vibrations mode .The optical results show that transmittance decreased drastically by increasing the doping ratio. In contrast with absorbance, it increased by increasing of the doping ratio of cerium oxide. The optical energy gap was found to change systematic sequence with increasing of CeO2 concentration. Also the optical constant with different CeO2 contents were determined..

Keywords: *Sno2:Pd Thin Films, Cerium Oxide, Optical Properties, Optical Constants FTIR .*

http://dx.doi.org/10.47832/2717-8234.18.26

[1] Ahmed.shaker1104a@sc.uobaghdad.edu.iq

[2] ghuson.mohammed@sc.uobaghdad.edu.iq

1. Introduction

The utilization of thin film semiconductors has sparked substantial interest in an expanding array of applications within diverse electrical and optoelectronic devices owing to their economical production costs, positioning thin film technology prominently in fundamental research. An analysis of the existing body of literature discloses that numerous scientific groups have delved into the realm of thin film technology. Consequently, a plethora of deposition techniques have been developed, the majority of which rely on continuous, high-temperature power sources [1]. Nanoparticles serve as the foundational building blocks in the field of nanotechnology, which showcases a myriad of applications across various domains like biosensors and electronic Nano devices [2]. A significant category of nanostructured materials pertains to the metal oxide thin films. The fabrication of nanomaterial's within thin films can be achieved through diverse methodologies. Numerous established techniques exist for the application of thin films onto a substrate, encompassing pulsed laser deposition [3], laser-induced plasma [4], chemical vapor deposition [5], reactive magnetron sputtering [6], spray pyrolysis [7], atomic layer deposition [8], Chemical bath deposition [9], among others. The utilization of wide-band gap oxides has been a persistent area of research due to their numerous functions and practical uses. [10] Because of its superior optical and electrical qualities, tin dioxide (SnO_2) is one of the functional oxides that is used widely in the areas of gas sensors, transparent conducting thin films, catalysis, solar cells, and other applications [11] SnO_2 does, however, have a broad direct bandgap of B3.6 eV [12]. It is well accepted that the dipole forbidden nature of SnO_2's band-edge quantum states makes it an unsuitable ultraviolet (UV) light emitter. [13]SnO_2's conduction-band minimum and valence-band maximum states exhibit even-parity symmetry, which hinders its potential employment in optical devices like photo detectors by preventing the band-edge radioactive transition and light emission [14]. Compared to other wide-bandgap oxides, where studies have shown the presence of UV emission in SnO_2, considerably less work has been done on the optical characteristics of SnO_2. [15] Although thin films are essential for device applications, the optical characteristics of SnO_2 thin films have only been the subject of a small number of studies to far[16].Cerium oxide (ceria) films have received considerable interest because of their high transparency in the visible and near IR region and electro-optical performance [17].It has potential applications in silicon-on-insulator structures, barrier layers and capacitor devices [18].It is a highly efficient UV absorber and is used as an additive for glass for protecting light-sensitive materials [19].Films are capable of corrosion protection of metals and as coating for use as a catalyst support [20].The ability of cerium-doped glass to block out UV light is utilized in the manufacturing of medical glassware and aerospace windows. It is also used to prevent polymers from darkening in sunlight and to suppress discoloration of television glass. In catalytic converters, it acts as a stabilizer for the high surface area alumina, as a promoter of the water–gas shift reaction and as an oxygen storage component.

2. Experimental

(2-1) Preparation of Samples

($SnO2_{0.9}$:$Pd_{0.1}$) powder with (99.99% purity) was mixed with different contents of CeO_2 nanoparticles (0.05, 0.10, 0.15, 0.20, 0.25)wt. The powder was gridded together for 10 minutes using a gate mortar. After that, it was compressed together with a hydraulic press under 5 tons pressure for (10 minutes) to have pellets of 1 cm diameter and 0.2 cm thickness. The pellets were sintered to (700°C) for one hour; after that, they were cooled to room temperature.

(2-2) Deposition of Thin Films

The prepared pellets were used to deposit $(SnO_2:Pd)_{1-x}CeO_{2x}$ thin films at room temperature on glass substrates with dimensions (2.5×7.5 cm) which were washed with distilled water using an ultrasonic procedure for 15 minutes. Thin films were prepared using the pulsed laser deposition technique employing Nd:YAG laser with a wavelength of (1064 nm) and energy 600 mJ, for 400 laser pulses, replicate frequency (6Hz) incident on the target surface with a 45 ° angle. The deposition was made at a chamber pressure of (1×10^{-1}) mbar. The target-substrate distance was 10cm. The film thickness was estimated using the interference method to be around 200±5 nm. After deposition of $(SnO_2:Pd)_{1-x}(CeO_2)_x$ the films were annealed to annealing temperature 673K for one hours in air.

(2-3)Measurements

The infrared (IR) spectrum of $(SnO_2:Pd)_{1-x}(CeO_2)_x$, films has been studied using a system equipped by the Japanese company the FTIR(IRAffinity-1-SHMADZU) for the spectrum range(400-4000)cm^{-1} , which is defined as the spectrophotometer for Fourier Transforms. The optical properties of thin films were studied using UV–Vis-NIR spectrophotometer (Metertech, SP8001) in the wavelength range of (400-1100) nm was analyzed to determine the refractive index, extinction coefficient, optical band- edge absorption coefficient and energy gap value for each sample.

3.Results and discussion

3.1 FTIR analysis

FTIR spectroscopy can be used for identification of the ionic and metal states in supported catalysts. Figure (1) shows the FTIR patterns for undoped and doped (SnO_2:Pd)thin films with different concentrations of CeO_2 content annealed to 673K. The specific peaks were identified and matched with the standard values done by previous researches. The strong band located at 640.32 $cm^{-1}$was assigned to the Ce-O stretching mode [13]. The weak band, corresponding to the Ce-O stretching mode of CeO_2 is seen at 500 cm^{-1}.The adsorption band at 1500 cm^{-1} can be attributed to N-O band and we

notice a weak peak at 1031.85 cm^{-1} belong to Ce-O attributed to H-O-H band. The strong absorption band at approximant 3429.20 cm^{-1} for all samples is attributed to the stretching mode of absorbed O-H .While the band at 1514.12 $cm^{-1}$are due to the existence of OH on the adsorbed water and Sn–OH. A sharp peak appeared at 2920.03 cm^{-1}due to carbon dioxide, which is incorporated from the atmospheric exposure. The broad band, corresponding to the Ce-O stretching mode of CeO_2 is seen at 500 cm^{-1}. It was noted that with the increase of the doping concentration, the infrared absorption becomes stronger [21].

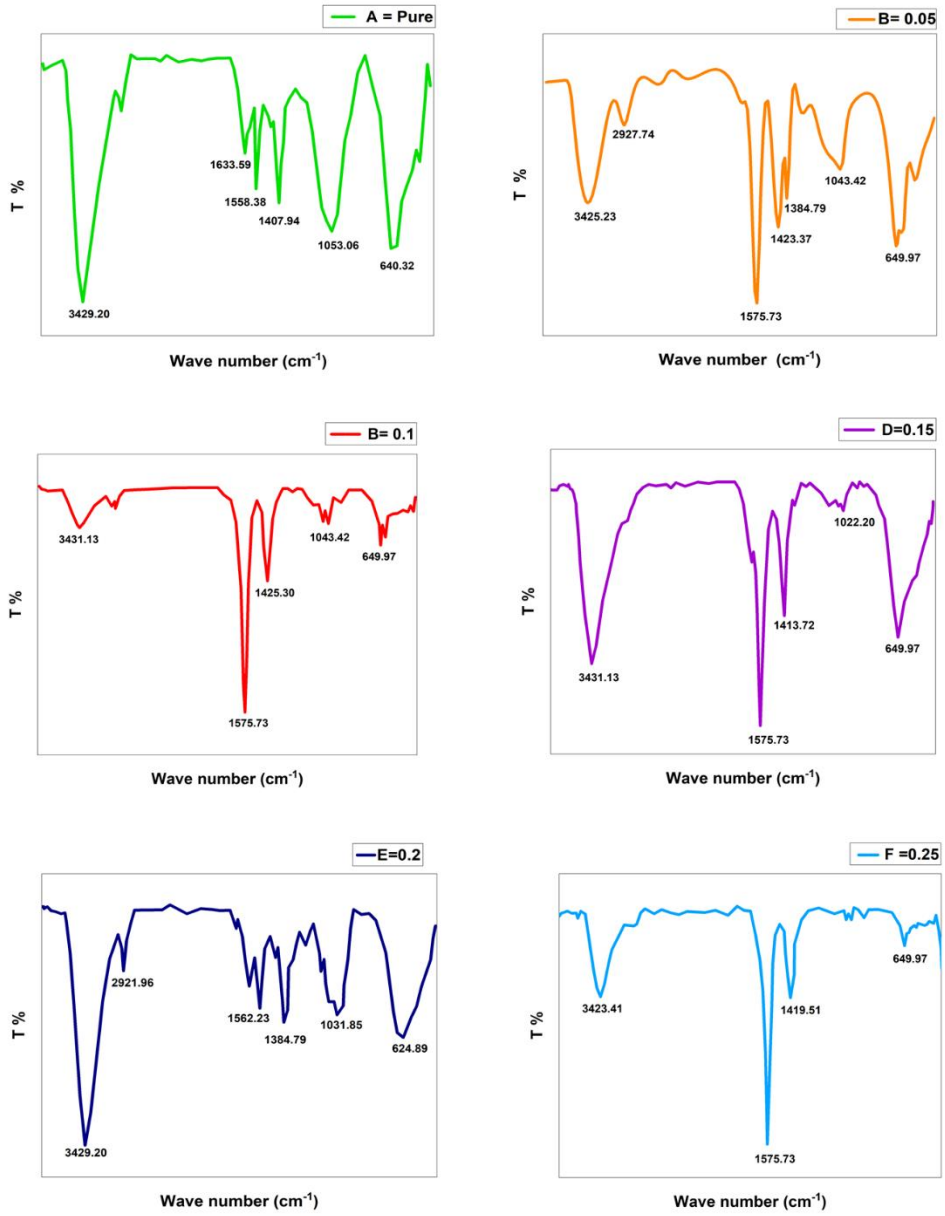

Figures (1) : FTIR for (SnO_2:Pd) thin films at wavelength (4000-400)cm^{-1} with different ratios of CeO_2 (A) x =0 (B) x = 0.05 (C) x = 0.10 (D)x=0.15 (E) x=0.2 and (F) x=0.25 prepared RT and annealed to 673K

3.2 Optical properties

3.2.1Transmittance (T)

Is given by the ratio of the intensity of the rays (I_T) transmitting through the film to the intensity of the incident rays (I_o) as follows:

$$T = (I_T / I_o) \quad \ldots\ldots\ldots\ldots\ldots\ldots\ldots\ldots\ldots \quad (1)$$

Figure (2) shows the optical transmittance spectra of undoped and doped SnO_2:Pd with different CeO_2 concentrations in the wavelength range of 400 nm to 1100 nm. The $(SnO_2{:}Pd)_{1-x}CeO_{2x}$ thin films that were made showed transparency in the visible spectrum, with an average transmittance of almost 88%, according to an analysis of the spectra shown in figure2. It is clear that a higher doping concentration caused the films' transmittance to decrease [22].

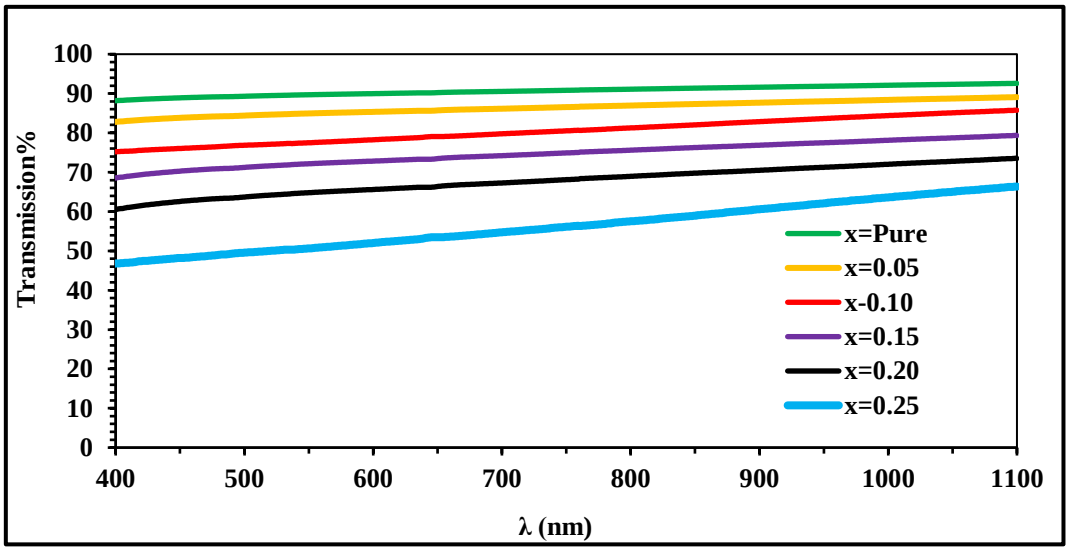

Figure(2) Transmittance as a function of wavelength for $(SnO_2{:}Pd)_{1-x}(CeO_2)_x$ thin films annealing to Ta=673K

3.2.2 Absorption Coefficient (α)

Absorption Coefficient (α) is stated as a rate, reducing in amount of fallen rays intensity respect to the distance unit in the way of fallen wave propagation in a specific medium. "α" reclines on incident photon energy (hν) and on semiconductor characteristics (n or p) kind, where electronic transitions are sorting (n) or (p) and forbidden energy gap. We can determine the photon energy by the relation as follows [23]:

$$E = h\nu \quad \ldots\ldots\ldots\ldots\ldots\ldots (2)$$

The photon will be transmitted through the material if the incident photon energy is less than the forbidden energy gap, the transmittance is given by the relation as follows:

$T = (1 - R)^2 \exp(-\alpha t)$ ……. (3)

where t is the thickness of the films, R is the reflectance

The absorption coefficient can be found through the relation:

$$\alpha = \frac{(2.303A)}{t} \quad \ldots\ldots\ldots (4)$$

Figure(3) shows the absorption coefficient (α) changes with a wavelength for annealed **$(SnO_2:Pd)_{1-x}$ $(CeO_2)_x$ films with different CeO_2 contents** .It has been observed that the values of the absorption coefficient are in the range (**$\alpha \geq 10^4$ cm^{-1}**). The values of the absorption coefficient of all samples are located within the high absorption zone. this helps to predict direct transitions within this range of energy also shows that the energy calculated at this point is the energy of a direct gap .Also Fig(3) show that the increase in the value of the absorption coefficient is almost linear in the visible region . In other words, when the concentration of CeO2 increases caused the films' transmittance to increase [24].

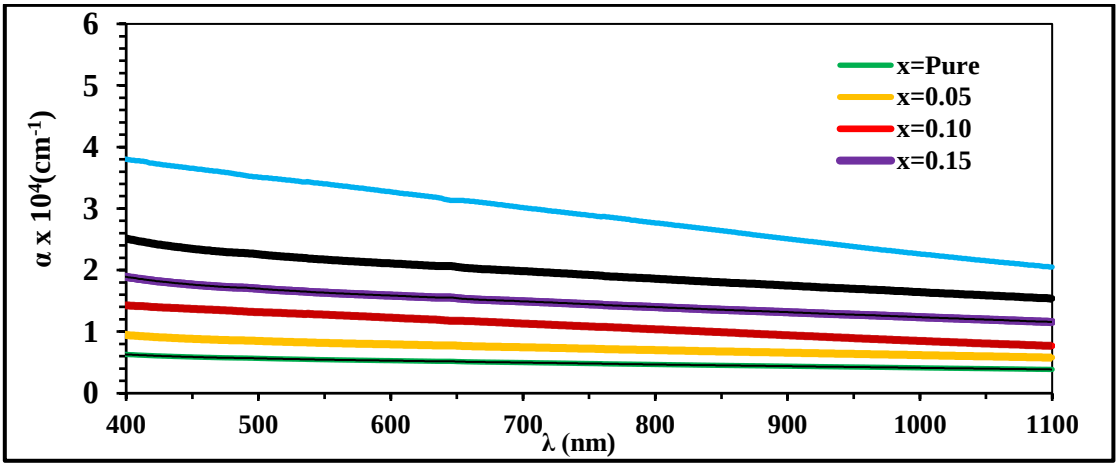

Figure (3) Absorption coefficient as a function of wavelength for SnO2:Pd)1-x (CeO2)x Thin Films annealed to 673K

The direct energy gap of SnO_2:Pd films with different CeO_2 content was calculated by drawing the relationship between **$(\alpha h\nu)$ $)^2$** and photon energy**$(h\nu)$** by drawing the straight part of the curve to cut the photon energy axis at the point [**$(\alpha h\nu)^2$**=0] we get the value of the forbidden energy gap for the allowed direct transition and Fig(4) shows variation between **$(\alpha h\nu)$ $)^2$** and photon energy**$(h\nu)$** for SnO_2:Pd films with different content of CeO_2 (0.05, 0.10, 0.15, 0.20, 0.25)Wt after annealing.

The effect of annealing temperatures on the value of Eg for (SnO_2:Pd) /CeO_2 films is presented in the Fig.(4).It can be observed that as the doping value increases, the energy gap values decrease. The decrease of Eg with the increase of CeO2 content (x) increases the

absorbance making the material opaque. This is due to the increase of the density of localized states in the Eg near valence band or conduction band, which are ready to receive electrons and generate tails in the optical energy gap reducing the energy gap. The decrease in the bandgap can also be correlated to many-body interaction effects, which occurs between either free carriers and ionized impurities or charge carriers [25]. Table 1 shows the bandgap values for the different CeO2 content

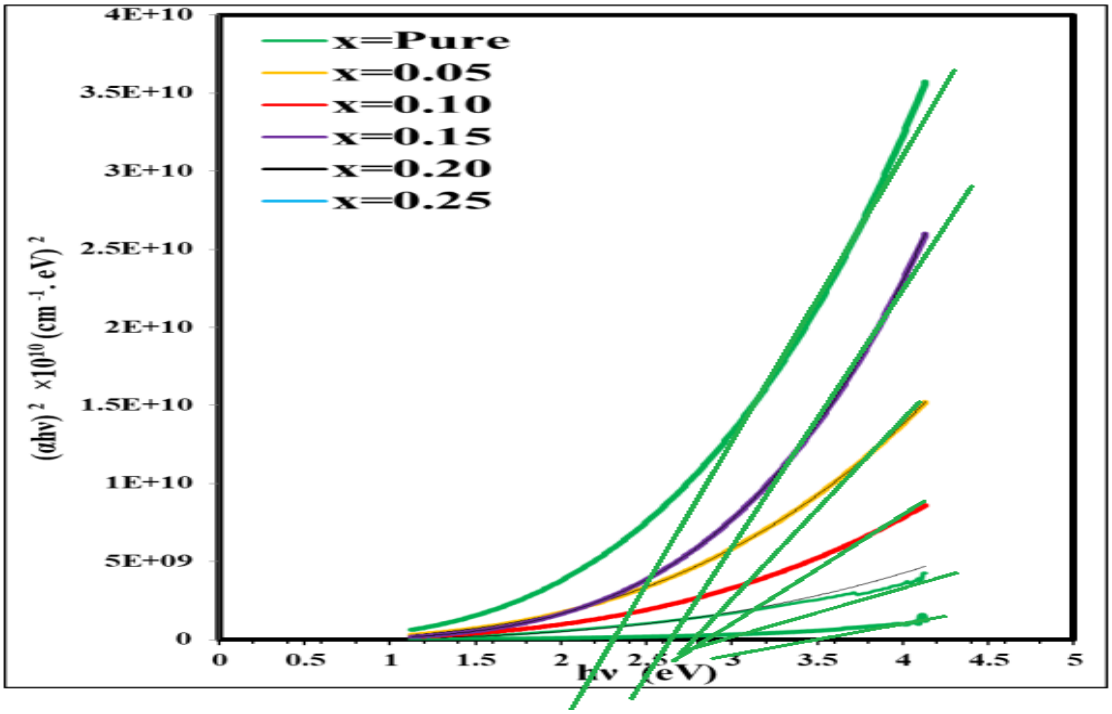

Figure (4). (ahv)² as a function of (hv) for $(SnO_2:Pd)_{1-x}$ $(CeO_2)_x$ films annealed to 673K

3.2.3 Refractive Index (n):

The refractive index can be defined as a ratio between the speed of light in vacuum (c), and the speed of light in the medium. The value of refractive index (n) is calculated by using equation depending on the reflectance and extinction coefficient (K_o) using the following equation:[22]

$$R = \frac{(n-1)2 + Ko\text{^}2}{(n+1)2 + Ko\text{^}2} \qquad \text{..... (5)}$$

Thus refractive index (n) is given by the following:[26]

$$n = \left[\frac{(1+R)^2}{(1-R)^2} - (k_o^2+1)\right]^{1/2} + \frac{(1+R)}{(1-R)} \qquad \text{.....(6)}$$

The variation of the refractive index with wavelength in the range (400–1100) nm for undoped and doped$(SnO_2:Pd)_{1-x}$ with different concentrations of CeO_2 films is illustrated in Figure (5). It can be noticed from this figure that the refractive index increases with increasing of concentration and the increase in refractive index can be ascribed to two

factors: a reduction in crystal size and a decrease in the band gap energy (Eg), which demonstrates an inverse correlation with the refractive index [25]. The values of refractive index are given in Table (1)

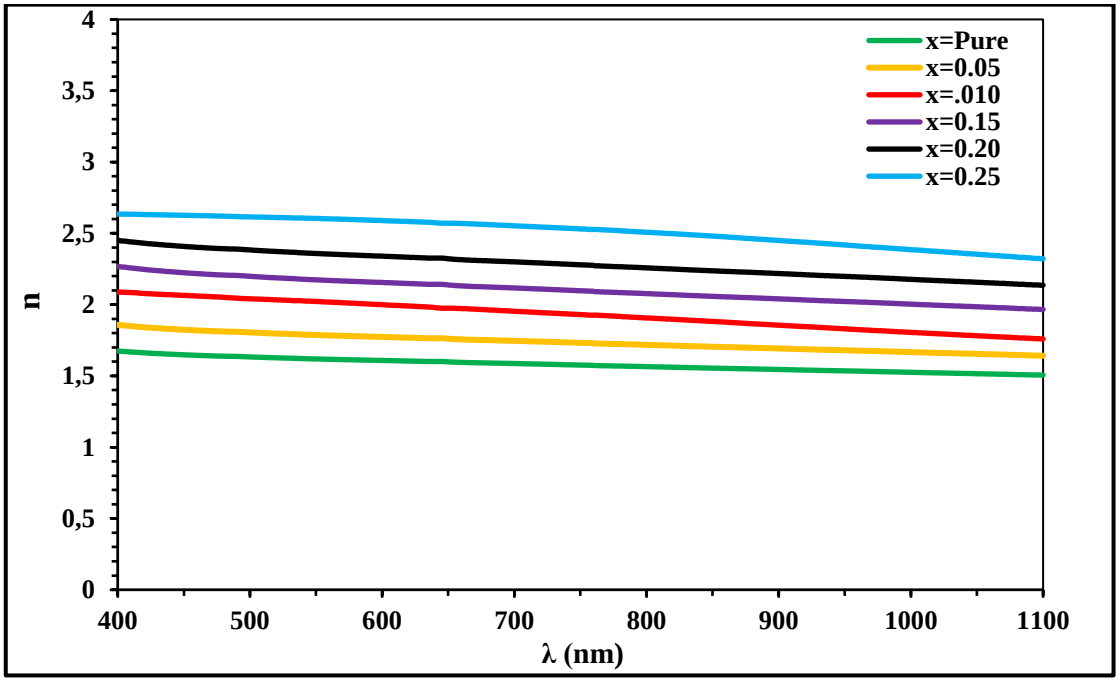

Figure (5) the variation of refractive index as a function of wavlength for SnO_2:Pd)$_{1-x}$ (CeO_2)$_x$ Thin films at different concentrations of CeO_2 annealed to 673K.

3.2.4Extinction coefficient (K_o):

The physical significance of (K_o) is best expressed by the fact that the intensity falls to exp(-2ωk_0x/c)of its initial value in propagating a distance through the medium.

It represents the imaginary part of complex refractive index (n*) as in the following equation

$$n^* = n + i K_o \quad \text{.....(7)}$$

Where: n: the real part of refractive index, n*: complex refractive index which depends on the material type, crystal structure (grain size), crystal defects, crystal stress. The extinction coefficient (K_o) is equal:

$$K_o = \alpha \lambda / 4\pi \quad \text{..... (8)}$$

Where λ: is the wavelength of incident rays.

The variation of the extinction coefficient with wavelength in the range of (400-1100) nm for (**SnO_2:Pd)1-x (CeO_2)x Thin Films** annealed to 673K is depicted in Figure (6). In general .it can be noticed from figure that the changes of the extinction coefficient follow the same changes of the absorption coefficient with the annealing temperature and doping

concentration. i.e the value of the extinction coefficient increases with increasing of CeO_2 content. [26]

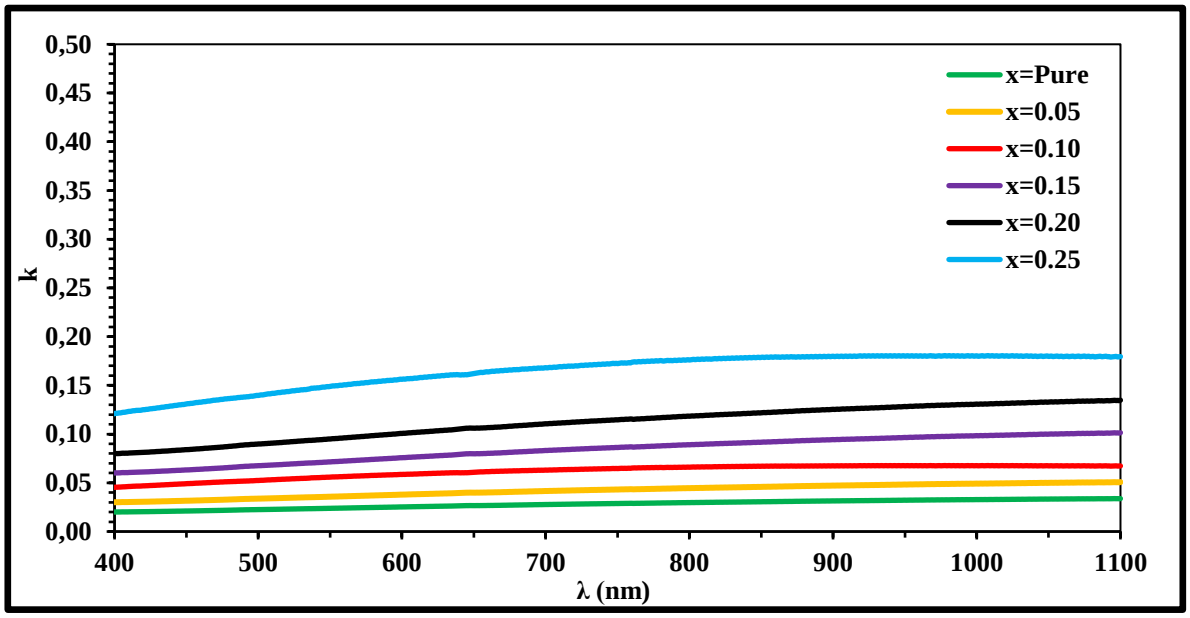

Figure (6) The variation of Extinction Coefficient as a function of wavelength for $(SnO_2:Pd)_{1-x}$ $(CeO_2)_x$ Thin Films annealed to 673K.

3.2.5 Dielectric Constant (ε):

The complex dielectric constant (ε) represents the ability of material to polarization, whose expression is given by the following equation: [27]

$$\varepsilon = (n^*)^2 = (n+iK_o)^2 \quad \text{.....(9)}$$

But the complex dielectric constant have two parts as [28]

$$\varepsilon = \varepsilon_1 + i\varepsilon_2 \quad \text{..... (10)}$$

Where ε_1 and ε_2 represents the real and imaginary parts of complex dielectric constant and they illustrated by the following relations [29]

$$\varepsilon_1 = (n^2 - K_o^2) \quad \text{..... (11)}$$

$$\varepsilon_2 = (2nK_o) \quad \text{..... (12)}$$

Figures (7) and (8) show the variation in the values of the real and imaginary part of the dielectric constant for the sample annealed to 673K. As the values of the real and imaginary part increases with increasing of CeO_2 content.

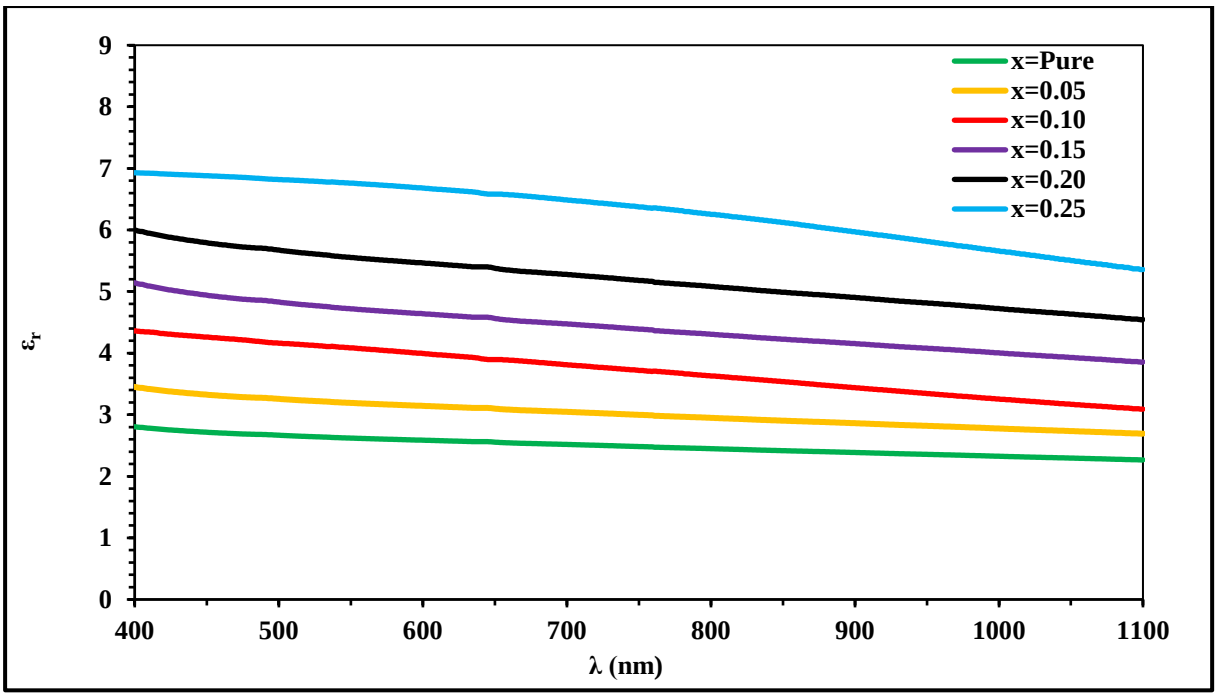

Figure (7) The ε_r as a function of wavelength for $(SnO2:Pd)_{1-x}$ $(CeO2)_x$ films annealed to 673K.

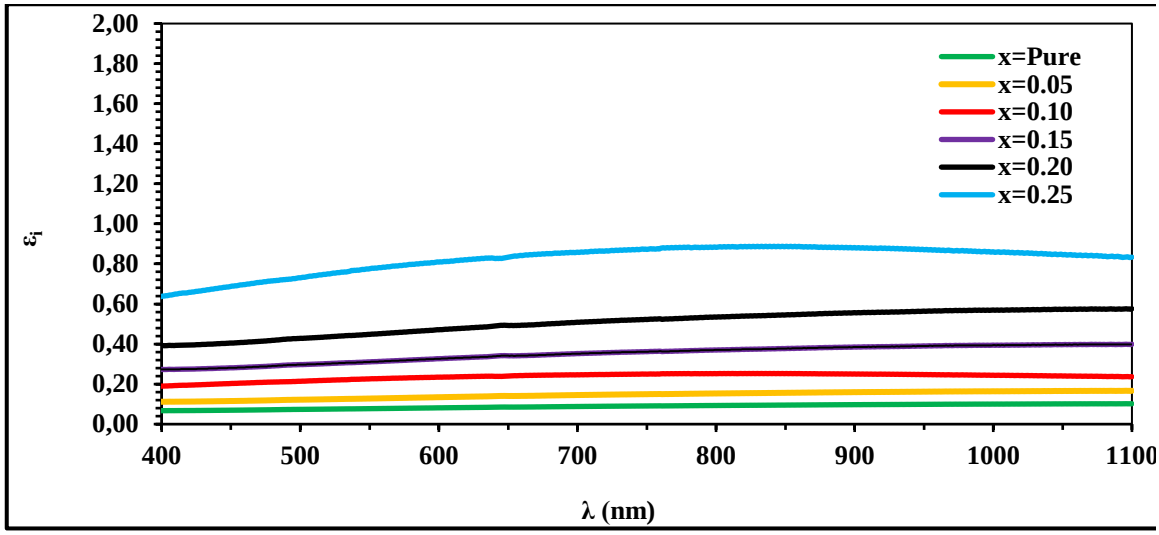

Figure (8) The εi as a function of wavelength for $(SnO_2: Pd)_{1-x}$ $(CeO_2)_x$ films annealed to 673K.

Table (1) : Reveals the transmittance spectra (T), refractive index (n), Absorption coefficient, Extinction coefficient (k), and Dielectric Constant of (SnO2:Pd)1-x (CeO2)x prepared for films annealed to 673 K at λ=500nm

Sample	T%	$\alpha*10^{-4}$ (cm^{-1})	k_{ex}	n	ε_r	ε_i	E_g(eV)
Pure	88.17	0.6295	0.020	1.675	2.804	0.067	3.4
0.05	82.79	0.9443	0.030	1.858	3.450	0.112	3.15
0.10	75.20	1.4250	0.045	2.089	4.360	0.190	2.8
0.15	68.54	1.8886	0.060	2.268	5.141	0.273	2.6
0.20	60.53	2.5103	0.080	2.450	5.999	0.392	2.5
0.25	46.77	3.8000	0.121	2.635	6.929	0.638	2.35

Conclusion

We have successfully prepared $(SnO_2:Pd)_{1-x}(CeO_2)_x$ films by PLD technique. From FTIR found the absorption peaks of (Sn-O) and peaks belong to CeO_2.The Optical studies of (SnO2:Pd)1-x $(CeO_2)x$ films in the wavelength range $400 < \lambda < 1110$ nm show that the material is highly transparent in the visible region. It also shows a lower reflectance in the ultra-violet region whereas a very high absorbance in this region. The optical band gap was found to decrease with increasing CeO_2 content. The values of absorption coefficient is found to increase with increasing CeO_2 content.

Reference

[1] P.U. Asogwa, S.C. Ezugwu, F.I. Ezema, "Variation of optical and solid state properties with post deposition annealing in PVA-Capped MnO2 thin films," Superficies y Vacio, 23(1) 18-22 (2010). https://www.fis.cinvestav.mx/~smcsyv/supyvac/23_1/SV2311810.pdf

[2] D.K. Naser, A.K. Abbas, and K.A. Aadim, "Zeta potential of Ag, Cu, ZnO, CdO and Sn nanoparticles prepared by pulse laser ablation in liquid environment," Iraqi Journal of Science, 2570-2581 (2020). https://doi.org/10.24996/ijs.2020.61.10.13

[3] R. Naeem, R. Yahya, A. Pandikumar, N.M. Huang, M. Misran, Z. Arifin, and M. Mazhar, "Photoelectrochemical properties of morphology-controlled manganese, iron, nickel and copper oxides nanoball thin films deposited by electric field directed aerosol assisted chemical vapor deposition," Materials Today Communications, 4, 141-148 (2015). https://doi.org/10.1016/j.mtcomm.2015.06.004

[4] Nadia Naeema, Ahmed Kudher and Ghuson H Mohammed "Study of the Spectroscopic Performance of Laser Produced CdTe, and CdTe:Ag Plasma" IOP Conf. Series: Materials Science and Engineering, 757 (2020) 012025 IOP Publishing doi:10.1088/1757-899X/757/1/012025

[5] Z.S. Mahdi, and G.H. Mohammed, "Structural and Optical Properties of GO-doped (TiO2: MoS2) Films Prepared by Pulsed Laser Deposition," Journal of Survey in Fisheries Sciences, 10(3S), 5658-5668 (2023).

https://sifisheriessciences.com/journal/index.php/journal/article/view/1954/2010

[6] F.K. Allah, S.Y. Abe, C.M. Nunez, A. Khelil, L. Cattin, M. Morsli, J.C. Bernede, et al., "Characterisation of porous doped ZnO thin films deposited by spray pyrolysis technique," Applied Surface Science, 253, 9241-9247 (2007).https://doi.org/10.1016/j.apsusc.2007.05.055

[7] O. Nilsen, H. Fjellvag, A. Kjekshus, "Growth of manganese oxide thin films by atomic layer deposition," Thin Solid Films, 444, 44-51 (2003). https://doi.org/10.1016/S0040-6090(03)01101-5

[8] H. Unuma, T. Kanehama, K. Yamamoto, K. Watanabe, T. Ogata, M. Sugawara, "Preparation of thin films of MnO2 and CeO2 by a modified chemical bath (oxidative-soak-coating) method," Journal of Materials Science, 38, 255-259 (2003). https://doi.org/10.1023/A:1021197029004

[9] M.A. Abood, and B.A. Hasan, "A Comparison Study the Effect of Doping by Ga2O3 and CeO2 On the Structural and Optical Properties of SnO2 Thin Films," Iraqi Journal of Science, 64(4), 1675-1690 (2023). https://doi.org/10.24996/ijs.2023.64.4.10

[10]3 Li, Y. F., Deng, R., Yao, B., Xing, G. Z., Wang, D. D. & Wu, T. Tuning ferromagnetism in MgxZn1-xO thin films by band gap and defect engineering. Appl. Phys. Lett. 97,102506 (2010).

[11] Qian, J., Liu, P., Xiao, Y., Jiang, Y., Cao, Y., Ai, X. & Yang, H. TiO2-coated multilayered SnO2 hollow microspheres for dye-sensitized solar cells. Adv. Mater. 21, 3663–3667 (2009).

[12] Snaith, H. J. & Ducati, C. SnO2-based dye-sensitized hybrid solar cells exhibiting near unity absorbed photon-to-electron conversion efficiency. Nano Lett. 10, 1259–1265 (2010).

[13]Li, Y., Deng, R., Tian, Y., Yao, B. & Wu, T. Role of donor-acceptor complexes and impurity band in stabilizing ferromagnetic order in Cu-doped SnO2 thin films. Appl. Phys. Lett. 100, 172402 (2012).

[14] Fro¨hlich, D., Kenklies, R. & Helbig, R. Band-gap assignment in SnO2 by two-photon spectroscopy. Phys. Rev. Lett. 41, 1750–1751 (1978).

[15] Yang, H. Y., Yu, S. F., Tsang, S. H., Chen, T. P., Gao, J. & Wu, T. High temperature excitonic lasing characteristics of randomly assembled SnO2 nanowires. Appl. Phys.Lett. 95, 131106 (2009).

[16] Divya Haridas, Vinay Gupta “Enhanced response characteristics of SnO2 thin film based sensors loaded with Pd clusters for methane detection” Sensors and Actuators B 166–167 (2012) 156–164, doi:10.1016/j.snb.2012.02.026

[17] Bandry P, Rodrigues A C M, Aegerter M A and Bulhoes L O 1990 J. Non-Cryst. Solids 121 319

[18] Brinker C J and Scherer G W 1990 Sol-gel science (New York: Academic Press) pp 180–184

[19] Bueno R M, Martinez-Duart J M, Hernández-Vélez M and Vaźquez L 1997 J. Mater. Sci. Eng. 32 1861

[20] A. Peng, Y. Gao, Q. Yang, X. Zuo, H. Tang, and G. Li, “MoC/MnO composite materials as high efficient and stable counter electrode catalysts for dye-sensitized solar cells,” Journal of Materials Science: Materials in Electronics, 31, 1976-1985 (2020). https://doi.org/10.1007/s10854-019-02717-8

[21]S. M. Sze, K. N. Kwok, "Physics of Semiconductor Devices," published simultaneously in Canada, vol. 978, pp. 750-4470, 2007

[22] Ahmad, A.; Alsaad, A.; Al-Bataineh, Q. Optical and structural characterization of dip synthesized Al-B CeO. Appl. Phys. A (2017) [104] S. Lany and A. Zunger, "Assessment of correction methods for the band-gap problem and for finite-size effects in supercell defect calculations: Case studies for ZnO and GaAs," Phys. Rev. B - Condens. Matter Mater.

[23]S. Sönmezoğlu, A. Arslan, T. Serin, and N. Serin, “The effects of film thickness on the optical properties of TiO2–SnO2 compound thin films,” Phys. Scr., vol. 84, no. 6, p. 65602, 2011

[24] G. Busch and H. Schade, Lectures on Solid State Physics: International Series in Natural Philosophy, vol. 79. Elsevier, 2013.

[25] Ö. A. Yildirim, H. E. Unalan, and C. Durucan, "Highly efficient room temperature synthesis of silver-doped zinc oxide (ZnO: Ag) nanoparticles: Structural, optical, and photocatalytic properties," J. Am. Ceram. Soc., Vol. 96, No. 3, pp. 766-773, (2013)

[26] S. J. Mousavi, ―First–Principle Calculation of the Electronic and Optical Properties of Nanolayered ZnO Polymorphs by PBE and mBJ Density Functionals,‖ J. Optoelectron. Nanostructures, vol. 2, no. 4, pp. 1–18, 2017

[27] I. Hassanien, A.S. Sharma, "Optical properties of quaternary a-Ge15-x Sbx Se50 Te35 thermally evaporated thin-films: Refractive index dispersion and single oscillator parameters. Optik, Vol. 200, pp. 163415, (2020)

[28] S. Sönmezoğlu, A. Arslan, T. Serin, and N. Serin, "The effects of film thickness on the optical properties of TiO2–SnO2 compound thin films," Phys. Scr. 84(6), 65602, 2011. https://doi.org/10.1088/0031-8949/84/06/065602

[29] Ali sh. Maktoof , Ghuson H. Mohamme "The Effect of Au Nanoparticles on the Structural and Optical Properties of (NiO:WO3) Thin Films Prepared by PLD Technique," Iraqi Journal of Science, 2022, Vol. 63, No. 6, pp: 2502-2513